Journal Name

ARTICLE TYPE

Cite this: DOI: 10.1039/xxxxxxxxxx

Distinguishing between heating power and hyperthermic cell-treatment efficacy in Magnetic Fluid Hyperthermia

Cristina Munoz-Menendez,[a] Ivan Conde-Leboran,[a] David Serantes,*[a,b] Roy Chantrell,[b] Oksana Chubykalo-Fesenko,[c] and Daniel Baldomir[a]

Received Date
Accepted Date

DOI: 10.1039/xxxxxxxxxx

www.rsc.org/journalname

In the *magnetic fluid hyperthermia* (MFH) research field it is usually assumed that achieving a uniform temperature enhancement (ΔT) of the entire tumour is a key-point for treatment. However, various experimental works reported successful cell apoptosis *via* MFH without noticeable ΔT of the system. A possible explanation of the success of those negligible-ΔT experiments is that a *local* ΔT restricted to the particle *nanoenvironment* (i.e. with no significant effect on the global temperature T) could be enough to trigger cell death. Shedding light on such possibility requires accurate knowledge of heat dissipation at local level in relation to the usually investigated *global* (average) one. Since size polydispersity is inherent to all synthesis techniques and heat released is proportional to particle size, heat dissipation spots with different performance -and thus different effect on the cells- will likely exist in every sample. In this work we aim for a double objective: 1- to emphasize the necessity to distinguish between total dissipated heat and hyperthermia effectiveness, and 2- to suggest a theoretical approach on how to select, for a given size polydispersity, the more adequate average size so that the most of the particles dissipate within a desired heating power range. The results are reported in terms of Fe_3O_4 nanoparticles as a representative example.

Magnetic fluid hyperthermia (MFH) is a promising technique for cancer treatment that uses the heat released by magnetic nanoparticles (MNPs) under an external AC field to treat the tumor.[1] Tumor cells are more sensitive to a temperature (T) rise than the healthy ones. Thus, MNPs can be delivered within the tumour for remotely-activated selective heating, avoiding undesired effects on the healthy tissue.

However, in spite of the big advancements achieved in the last years (even reaching clinical application[2]), MFH has not attained its anticipated full potential as complement/alternative to usual cancer treatment techniques. Intense research activity is therefore devoted to enhance the efficacy of MFH. This constitutes a complex task that requires combined work from different areas of knowledge; ranging from chemistry, biology, and medicine (MNP synthesis, biocompatibility, clinical needs);[3,4] to physics and engineering (precise heating, human-sized AC field devices).[1,5] Achieving accurate heating performance is the subject of the present work.

A large number of research works investigating MFH seeks the optimum conditions (particle size,[6] anisotropy,[7] etc.), giving the largest heating power. That is to say, they implicitly assume a direct correlation between dissipated power and efficacy of MFH to treat the tumor: the higher the heating, the more effective the treatment is. The problem is that such an approach cannot explain the several times reported occurrence of hyperthermia induced cell death under negligible temperature rise.[8,9] In fact, what these results suggest is that heating only the particle's *nanoenvironment* could be enough to trigger the cell apoptosis, thus casting doubt on the usually presumed need of a large temperature increase (ΔT) of the overall system for an efficient MFH treatment. This interpretation finds support in the sharp temperature profiles observed in the close nanoenvironment of the MNPs during exposure to an AC field,[10] where the ΔT increases achieved at the nanoparticle surface (of several tens of K), rapidly decay to zero only a few nanometers away. Such huge ΔT values would likely damage the cells and induce apoptosis without noticeable changes in the global temperature. Stress-induced gene expres-

[a] *Instituto de Investigacións Tecnolóxicas and Departamento de Física Aplicada, Universidade de Santiago de Compostela, 15782 Santiago de Compostela, Spain*
[b] *Department of Physics, University of York, York YO10 5DD, U.K.*
[c] *Instituto de Ciencia de Materiales de Madrid, CSIC, Cantoblanco, ES-28049 Madrid, Spain*
* Corresponding author: david.serantes@usc.es

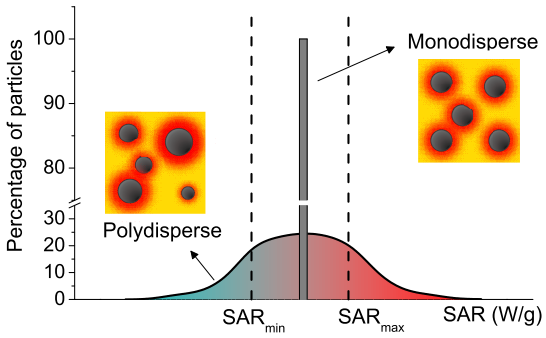

Fig. 1 (Color online) Example histogram comparing the heating performance of a monodisperse and a polydisperse system. Vertical dashed lines stand for safety boundaries to avoid infra/overheating (SAR_{min} and SAR_{max}, respectively).

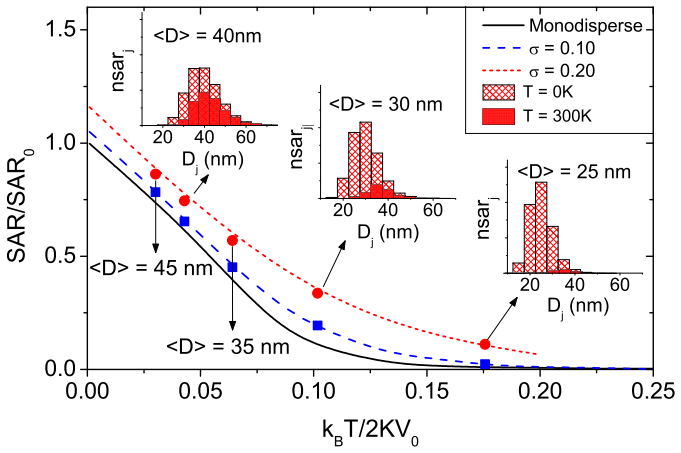

Fig. 2 Dimensionless SAR/SAR_0 values for different σ and for different thermal fluctuation conditions as described by $k_BT/2KV_0$. In both cases the 0-subindex stands for the equivalent monodisperse case. The arrows indicate the average sizes of Fe_3O_4 NPs having such SAR values at $T = 300\,K$. The histograms show the heating performance ($\frac{N_j}{N} \cdot SAR_j = nsar_j$ values) for the different sizes within a given sample ($\sigma = 0.20$) and for different $\langle D \rangle$ values.

sion sensing has recently being reported by de Sousa *et al.*[11] as a promising methodology to investigate local heating within cells.

The above arguments clearly emphasize the need to redirect/expand efforts in the MFH research roadmap: the study of the overall heating performance of the system must be accompanied by an accurate knowledge of the released heat at local level. In this regard it is essential to take into account the size distribution inherent to any synthesis technique. The heating performance of the MNPs, characterized in terms of the *Specific Absorption Rate* (SAR, in W/g_{MNP} units), is proportional to the particle size. Hence, MNPs of different size will behave as local heat dissipation spots with different performance (see Fig. 1), and consequently will have a different effect on the surrounding tissue. Note that while overheating may cause undesired effects (for example damage on the healthy tissue or necrotic cell death), infra-heating may leave the malignant cells unharmed and thus make the treatment ineffective. In the present work we present a theoretical approach on how to choose a particle system so that most of the particles dissipate within a desired treatment range $SAR_{treat} \in [SAR_{min}, SAR_{max}]$, where SAR_{min}, SAR_{max} correspond to minimum and maximum SAR values to avoid infra- and overheating, respectively. This is illustrated in Fig. 1.

Our approach is based on correlating the heating properties at *global* (average system) and *local* (single particle) levels, following the procedure described in Ref. 12. Since we consider the usual lognormal distribution in particle diameters (D) with standard deviation σ, we aim to correlate local and global SAR with the average nanoparticle diameter, $\langle D \rangle$, and a given σ. Based on their suitability for biomedical use,[3] we have used the characteristics of Fe_3O_4 MNPs as a paradigmatic example.

We used the Monte Carlo method[5,12] to simulate magnetization *vs.* field $M(H)$ loops to obtain $SAR = A \cdot f$, where A is the loop area and f the frequency of the H_{AC} field. The experimental conditions considered were $T = 300\,K$, $f = 500\,kHz$ and H_{AC} field amplitude of $H_{max} = 300\,Oe$. For the Fe_3O_4 MNPs we assumed density $\rho = 5.2\,g/cm^3$ and saturation magnetization $M_S = 480\,emu/cm^3$ at room temperature.[13] The anisotropy constant was approximated as an effective uniaxial one, of value $K = 14400\,erg/cm^3$ as in Ref. 14. This value is very close to the usual uniaxial approximation[15,16] of cubic anisotropy (K_C), i.e. $K = |K_C|/12$. To simplify the interpretation of the results we assumed non-interacting conditions. $\langle D \rangle$ and σ were systematically varied. To compare with the overall heating properties of the entire system, the local values are grouped by size and indicated by a j subscript. Thus, the sample follows a discrete lognormal distribution in diameters, grouped into categories, where each one of the categories j have N_j particles of size D_j and releases SAR_j. Once we know the SAR_j values, and since we also know the size distribution, we can calculate the percentage of particles releasing certain energy between the desired SAR_{min} and SAR_{max} values thanks to the cumulative frequency. Doing so for various $\langle D \rangle$ and σ allows to select the most convenient average size so that the majority of the particles are releasing between the desired SAR_{min} and SAR_{max}.

The first issue to investigate is the influence of choosing a system with a larger or smaller $\langle D \rangle$ value on the heating at global (overall SAR) and local (distribution of heat spots) levels. Note that the assumed conditions correspond to major loops ($H_{max} > H_A$, where $H_A = 2K/M_S$ is the anisotropy field of the MNPs and K is size-independent) for all particles. Thus the heating performance of particles with different sizes will be only determined by the relative robustness to thermal energy, which can thermally drive transitions over the anisotropy energy barrier.

The effect of thermal fluctuations on the average SAR for different $\langle D \rangle$ values is illustrated in Fig. 2 for different σ conditions. The results are presented in normalized units of SAR/SAR_0 and $k_BT/2KV_0$, where the 0-subindex stands for the monodisperse case, both for SAR and volume (V). As expected, increasing thermal fluctuations leads to a decrease in the heating output. On the other hand, a larger σ increases the overall SAR value for a fixed $\langle D \rangle$. This is because increasing the standard deviation in diameters results in an increase of the average volume[12] (note that $\langle V \rangle = V_0 \cdot e^{3\sigma^2}$). Therefore, given that bigger particles are able to release more energy, it is clear that a system with a larger σ will have a larger <V> and therefore a higher global SAR. The system

becomes more stable against thermal fluctuations.

Regarding the *local* level, the insets are histograms depicting the local heating for a sample with a fixed $\sigma = 0.20$ and different $\langle D \rangle$ values. Each histogram shows the performance at $T = 300\,K$ in comparison with the highest achievable one (at $T = 0\,K$). The three representative examples point out the size-dependent influence of thermal fluctuations, more pronounced in the smaller size categories. In fact, negligible contribution of the smaller sizes for $\langle D \rangle = 25\,nm$ is observed. This behavior could apparently be beneficial: less dispersion of local *SAR* values is *a priori* more desirable for MFH purposes. However, the marked decrease of the overall *SAR* might fall below the minimum MFH treatment requirements (SAR_{min}). It is therefore important to have access to a detailed analysis, correlating the heating performance at both *global* and *local* levels.

A more quantitative approach to the problem is depicted in Fig. 3, where the percentage of particles dissipating as a function of local *SAR* (black squares) is presented together with the cumulative frequency (blue triangles). Three representative cases, $\langle D \rangle =$ 30, 40, and 50 nm, and $\sigma = 0.20$ are shown for illustrative purposes. It is observed that the peak percentage, $\%_p$, shifts to higher *SAR* values for samples with larger $\langle D \rangle$, reflecting the higher stability against thermal fluctuations. However, its absolute value decreases and local heating performance broadens. The choice of the mean diameter $\langle D \rangle$ cannot be determined, therefore, as the one generating the highest $\%_p$. It needs to be correlated to that having the larger fraction of particles dissipating within a given SAR_{treat} range. This information can be obtained *via* the cumulative frequency (CF) data.

The CF data for the different $\langle D \rangle$ values show different shapes depending on the sample mean diameter: rapid growth and saturation for small $\langle D \rangle$; or moderate initial increase followed by a pronounced growth, before saturation occurring for large $\langle D \rangle$. Such particular shape points out the most adequate $\langle D \rangle$ to be the one for which the fast-growth range of the CF overlaps with the desired SAR_{treat} range. Two different SAR_{treat} examples (both of same $50 W/g$ width) are depicted in Fig. 3 as vertical shadowed areas. The % of particles falling within the SAR_{treat} range is written for each $\langle D \rangle$ case. It is observed that even though σ is the same for all cases, the amount of particles releasing energy in a desired *SAR* range significantly varies with $\langle D \rangle$. In addition, the values falling within each range are in general quite low, with wide dispersion of heating power for all cases. This emphasizes the relevance of correlating the heating performance at local level with the overall response of the system.

The systematic results of the percentage of particles dissipating within given *SAR* values (in intervals of $50\,W/g$) are reported in Fig. 4. Two different σ values are considered and the average size of the particles is varied at $5\,nm$ intervals. Also, the average *SAR* values of the entire system are shown. It seems clear from the plotted data that, depending on the required working SAR_{treat} range, a different $\langle D \rangle$ will be optimal. In general, local SAR_j values spread with increasing σ and $\langle D \rangle$. Higher $\langle D \rangle$ allow to have more particles dissipating in a higher SAR_{treat} range. Smaller $\langle D \rangle$ may help to have more dissipation in a narrower SAR_{treat} range.

Fig. 4 provides a guideline on how to choose the average parti-

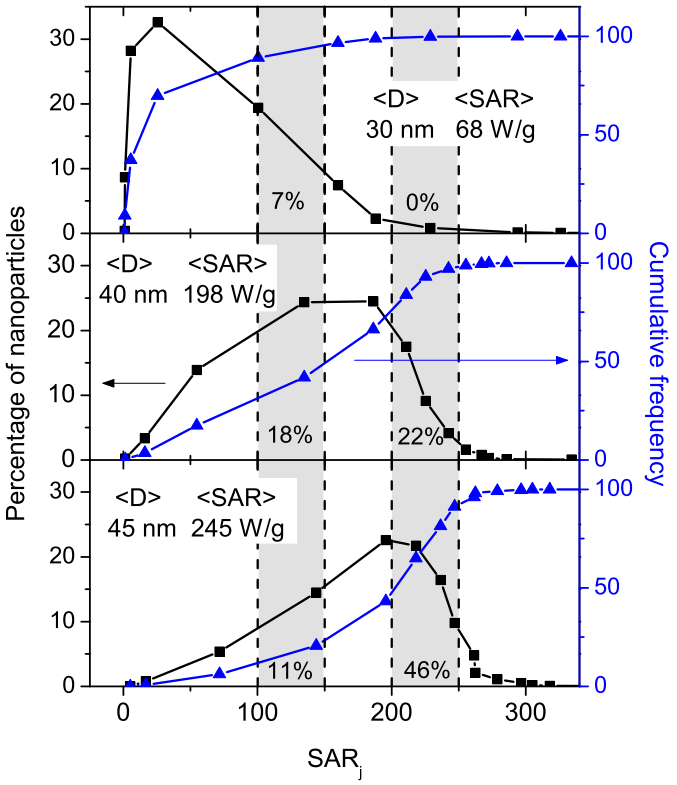

Fig. 3 Percentage of particles dissipating certain power SAR_j (black squares) for three illustrative cases of $\langle D \rangle = 30$, 40, and 45 nm magnetite particles. The right axis stands for the corresponding cumulative frequency data (blue triangles). Vertical shadowed regions illustrate how the amount of particles dissipating within a given SAR_{treat} range varies with $\langle D \rangle$. The vertical red full line shows the mean *SAR* for the corresponding sample.

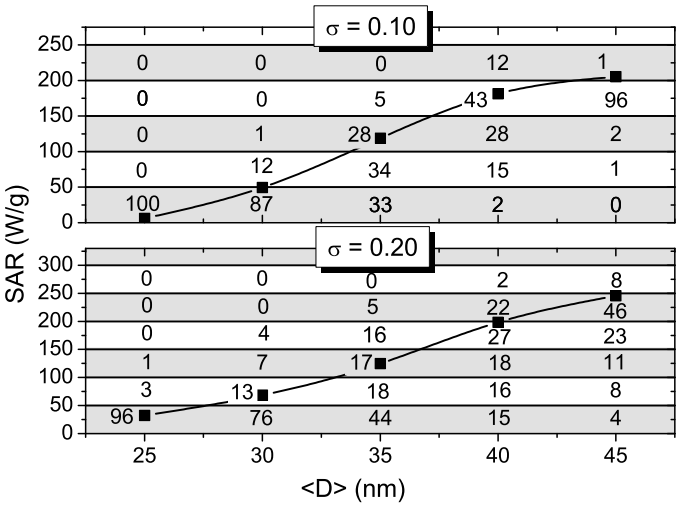

Fig. 4 Percentage of magnetite particles dissipating within a given *SAR* range (at $50 W/g$ intervals) as a function of the average particle diameter $\langle D \rangle$. Two different σ cases are considered. The black squares correspond to the average *SAR* in each case (the black line joining them is just a guide to the eye).

cle size that allows having the biggest number of particles releasing in the *SAR* range of interest. For example, let us consider that the tissue intended to be subjected to hyperthermia treatment had a optimum SAR of about $60\,W/g$. Looking at global *SAR* values, the most suitable particles would be those with $\langle D\rangle = 30\,nm$ and $\sigma = 0.20$. However, a detailed analysis of the local values shows that about 76% of the particles would be dissipating below $50\,W/g$, likely being ineffective for the treatment. Thus, for this particular example it would seem more effective to use $\langle D\rangle = 35\,nm$ and $\sigma = 0.10$ nanoparticles, which despite of having a much larger global *SAR* (of about $120\,W/g$, *i.e.* double), would have about one third of the system locally dissipating in a closer heating range.

In conclusion, we have shown the necessity to distinguish between global heating and cell-treatment efficacy for improved hyperthermia treatment. In this regard, we have suggested a theoretical approach on how to make the selection of the particle system properties (average size and size dispersion) for having the majority of the particles dissipating into a desired SAR range. This can be done by using the cumulative frequency to account for the fraction of particles within the sample dissipating certain SAR_j values within the desired SAR_{treat} range. It is important to emphasize, however, that the analysis reported here only deals with heat dissipation properties, not taking into account the rate of released heat to the environment. This is an important aspect, not considered in most of modelling studies so far, to be developed in the future, since the local differences in heat will be also influenced by a variety of factors such as, *i)* thermal conductivity and diffusion rate; *ii)* relative distance and spatial arrangement on the particles; *iii)* presence of heat sinks. Finally, it is also worth to recall the the main goal of the present work was to highlight the general need to account for *local* heating effects in MFH, and not to solve a specific case. Therefore it will be necessary to generalize the results in order to be able to predict the behavior of any type of particle (the ones reported are just one example for a particular combination of K and M_S). It will be particularly challenging to extend the study to systems with a dispersion of K values, what likely results in fractions of the system undergoing minor-cycle conditions;[15] and also to address the role of interparticle dipolar interactions.[5]

The authors thank the Centro de Supercomputación de Galicia (CESGA) for the computational facilities. This work was co-financed by the Spanish MINECO (Project MAT2013-47078-C2-2-P) and Xunta de Galicia, Spain (Project GRC 2014/013 and financial support of D.S. under Plan I2C).

References

1 E. A. Périgo, G. Hemery, O. Sandre, D. Ortega, E. Garaio, F. Plazaola and F. J. Teran, *App. Phys. Rev.*, 2015, **2**, 041302.
2 *MagForce Nanotechnologies AG, Berlin, Germany*, http://www.magforce.de/en/home.html, 2016.
3 M. Colombo, S. Carregal-Romero, M. F. Casula, L. Gutiérrez, M. P. Morales, I. B. Böhm, J. T. Heverhagen, D. Prosperi and W. J. Parak, *Chem. Soc. Rev.*, 2012, **41**, 4306–4334.
4 M. Mahmoudi, S. Sant, B. Wang, S. Laurent and T. Sen, *Adv. Drug Deliv. Rev.*, 2011, **63**, 24–46.
5 I. Conde-Leboran, D. Baldomir, C. Martinez-Boubeta, O. Chubykalo-Fesenko, M. P. Morales, G. Salas, D. Cabrera, J. Camarero, F. J. Teran and D. Serantes, *J. Phys. Chem. C*, 2015, **119**, 15698–15706.
6 G. Salas, J. Camarero, D. Cabrera, H. Takacs, M. Varela, R. Ludwig, H. Dähring, I. Hilger, R. Miranda, M. del Puerto Morales and F. J. Teran, *J. Phys. Chem. C*, 2014, **118**, 19985–19994.
7 S. Ruta, R. Chantrell and O. Hovorka, *Sci. Rep.*, 2015, **5**,.
8 M. Creixell, A. C. Bohorquez, M. Torres-Lugo and C. Rinaldi, *ACS Nano*, 2011, **5**, 7124–7129.
9 A. Villanueva, P. De La Presa, J. Alonso, T. Rueda, A. Martinez, P. Crespo, M. P. Morales, M. Gonzalez-Fernandez, J. Valdes and G. Rivero, *J. Phys. Chem. C*, 2010, **114**, 1976–1981.
10 J. T. Dias, M. Moros, P. del Pino, S. Rivera, V. Grazú and J. M. de la Fuente, *Angew. Chem.*, 2013, **125**, 11740–11743.
11 M. E. de Sousa, A. Carrea, P. Mendoza Zélis, D. Muraca, O. Mykhaylyk, Y. E Sosa, R. G Goya, F. H. Sanchez, R. A Dewey and M. B. Fernández van Raap, *J. Phys. Chem. C*, 2016.
12 C. Munoz-Menendez, I. Conde-Leboran, D. Baldomir, O. Chubykalo-Fesenko and D. Serantes, *Phys. Chem. Chem. Phys.*, 2015, **17**, 27812–27820.
13 K. J. Klabunde, *Nanoscale materials in chemistry*, Wiley Online Library, 2001.
14 C. Martinez-Boubeta, K. Simeonidis, D. Serantes *et al.*, *Adv. Funct. Mater.*, 2012, **22**, 3737–3744.
15 G. Vallejo-Fernandez and K. O'Grady, *Appl. Phys. Lett.*, 2013, **103**, 142417.
16 N. Usov, S. Gudoshnikov, O. Serebryakova, M. Fdez-Gubieda, A. Muela and J. Barandiarán, *J. Supercond. Nov. Magn.*, 2013, **26**, 1079–1083.